Journal of Physics D: Applied Physics

ACCEPTED MANUSCRIPT

Ni Schottky barrier on heavily doped phosphorous implanted 4H-SiC

To cite this article before publication: Marilena Vivona *et al* 2021 *J. Phys. D: Appl. Phys.* in press https://doi.org/10.1088/1361-6463/ac13f3

Manuscript version: Accepted Manuscript

Accepted Manuscript is “the version of the article accepted for publication including all changes made as a result of the peer review process, and which may also include the addition to the article by IOP Publishing of a header, an article ID, a cover sheet and/or an ‘Accepted Manuscript’ watermark, but excluding any other editing, typesetting or other changes made by IOP Publishing and/or its licensors”

This Accepted Manuscript is **© 2021 IOP Publishing Ltd**.

During the embargo period (the 12 month period from the publication of the Version of Record of this article), the Accepted Manuscript is fully protected by copyright and cannot be reused or reposted elsewhere.
As the Version of Record of this article is going to be / has been published on a subscription basis, this Accepted Manuscript is available for reuse under a CC BY-NC-ND 3.0 licence after the 12 month embargo period.

After the embargo period, everyone is permitted to use copy and redistribute this article for non-commercial purposes only, provided that they adhere to all the terms of the licence https://creativecommons.org/licences/by-nc-nd/3.0

Although reasonable endeavours have been taken to obtain all necessary permissions from third parties to include their copyrighted content within this article, their full citation and copyright line may not be present in this Accepted Manuscript version. Before using any content from this article, please refer to the Version of Record on IOPscience once published for full citation and copyright details, as permissions will likely be required. All third party content is fully copyright protected, unless specifically stated otherwise in the figure caption in the Version of Record.

View the article online for updates and enhancements.

This content was downloaded from IP address 150.145.42.11 on 14/07/2021 at 09:49

IOP Publishing Journal Title
Journal XX (XXXX) XXXXXX https://doi.org/XXXX/XXXX

1
2
3
4
5
6
7
8
9
10
11
12
13
14
15
16
17
18
19
20
21
22
23
24
25
26
27
28
29
30
31
32
33
34
35
36
37
38
39
40
41
42
43
44
45
46
47
48
49
50
51
52
53
54
55
56
57
58
59
60

Ni Schottky barrier on heavily doped phosphorous implanted 4H-SiC

M Vivona, G Greco, M Spera, P Fiorenza, F Giannazzo, A La Magna and F Roccaforte

Consiglio Nazionale delle Ricerche – Istituto per la Microelettronica e Microsistemi (CNR_IMM), Strada VIII, n. 5 Zona Industriale, 95121 Catania, Italy

E-mail: marilena.vivona@imm.cnr.it

Received xxxxxx
Accepted for publication xxxxxx
Published xxxxxx

Abstract

The electrical behavior of Ni Schottky barrier formed onto heavily doped (N_D>10^{19} cm^{-3}) n-type phosphorous implanted silicon carbide (4H-SiC) was investigated, with a focus on the current transport mechanisms in both forward and reverse bias. The forward current-voltage characterization of Schottky diodes showed that the predominant current transport is a thermionic-field emission mechanism. On the other hand, the reverse bias characteristics could not be described by a unique mechanism. In fact, under moderate reverse bias, implantation-induced damage is responsible for the temperature increase of the leakage current, while a pure field emission mechanism is approached with bias increasing. The potential application of metal/4H-SiC contacts on heavily doped layers in real devices are discussed.

Keywords: 4H-SiC, electrical characterization, current transport, Schottky device

1. Introduction

In last decades, wide-bandgap semiconductors have attracted great interest for the development of high-power electronic devices and systems [1,2]. The interest towards these materials is based on their extraordinary physical and electronic properties, such as a wide bandgap, high breakdown electric field strength, high saturation electron velocity and high thermal conductivity [3]. Particularly, the hexagonal polytype of silicon carbide (4H-SiC) plays a pivotal role thanks to the maturity reached in terms of material quality and technological implementation of the device fabrication steps [4]. In fact, 4H-SiC unipolar devices, such as Schottky barrier diodes (SBDs) and metal-oxide-semiconductor field effect transistors (MOSFETs), with high performances (low on-state voltage drop, high breakdown voltage, high switching speed, possibility to operate at high temperature, etc.), have become largely available on the market [4,5,6].

However, in order to fully exploit the potentialities of this material, significant efforts are currently devoted to address some physical concerns, which still limit the performances of SiC devices [7]. For SiC devices, a full understanding of the Schottky barriers properties is particularly useful in several applications. For example, while in SBDs used as sensors and detectors a high Schottky barrier height is desired [8,9], a reduction of the barrier is targeted in power electronics applications to minimize the device power consumption [10]. Typically, the Schottky barrier properties can be tailored by an optimized choice of metal (e.g., low work-function metals, tunable compositions, etc.) [11,12,13,14], by suitable semiconductor surface treatments [15,16] or by intentionally changing the electric field distribution below the interface by ion-irradiation [17]. In this context, many efforts have been dedicated to the basic understanding of the current transport in metal/semiconductor contacts on both lightly- and heavily-doped epitaxial 4H-SiC layers [18,19,20]. On the other hand,

Accepted Manuscript

 © xxxx IOP Publishing Ltd

1 2 3 4 5 6 7 8 9 10 11 12 13 14 15 16 17 18 19 20 21 22 23 24 25 26 27 28 29 30 31 32 33 34 35 36 37 38 39 40 41 42 43 44 45 46 47 48 49 50 51 52 53 54 55 56 57 58 59 60

ion implantation is used to form heavily-doped n-type and p-type regions in junction barrier Schottky (JBS) rectifiers and MOSFETs for the creation of Ohmic contacts [21,22,23]. On such implanted layers, Ohmic contacts can be formed by annealing at high temperature (> 900°C) of Nickel films, owing to the formation of nickel silicide (Ni_2Si) [23,24]. Hence, the knowledge of the carrier transport mechanisms at metal/heavily-doped SiC interfaces is a fundamental issue for the optimization of the contacts in these SiC devices. Recently, Hara et al. [25] studied the forward carrier transport mechanism in Schottky diodes fabricated on 4H-SiC epitaxial layers with different donor concentrations (up to a doping concentration as high as 1.8×10^{19} cm^{-3}), observing a reduction of the barrier height with increasing the epilayer doping.

In this work, the electrical behavior of Ni Schottky contacts onto heavily doped ($N_D > 10^{19}$ cm^{-3}) n-type phosphorus-implanted 4H-SiC was investigated, in both forward and reverse bias. Specifically, a reduced turn-on voltage was achieved under forward bias, where the thermionic field emission mechanism dominates the current transport through the interface. On the other hand, the behavior of the contact under reverse bias was explained considering a tunneling mechanism assisted by the presence of ion-implantation-induced defects for moderate reverse bias, while probably approached a pure field emission regime with bias increasing. Finally, a numerical simulation of the potential distribution in a JBS diode structure demonstrated the feasibility of this approach in real devices.

2. Experimental details

The material used in our study was a n-type 4H-SiC epitaxial layer (with nitrogen doping of 1×10^{16} cm^{-3}) grown onto a heavily doped 4H-SiC (0001) substrate. First, the upper part of the epitaxial layer was implanted at 400 °C using phosphorus (P) ions at energies ranging from 30 to 200 keV and with ion doses between 7.5×10^{13} – 5×10^{14} cm^{-2}. In this way, an implantation profile extending over 200 nm and with a peak concentration of 1×10^{20} cm^3 is obtained, as confirmed by secondary ion mass spectrometry (SIMS) reported in ref. [26], that also showed a structural investigation by cross-section transmission electron microscopy (TEM) analysis. Then, a post-implantation thermal annealing treatment was carried out at 1675 °C in Ar ambient, protecting the surface with a carbon capping layer [27], in order to achieve the electrical activation of the dopant.

Schottky barrier diodes were fabricated on this material. Before the front-side processing of the sample, a large-area back-side contact was fabricated by Ni-deposition followed by rapid thermal annealing (RTA) at 950 °C in N_2-atmosphere [23]. Successively, a 100 nm-thick Ni-layer was deposited on the P-implanted surface by direct current (DC) magnetron sputtering and defined in circular structures (radius of 250 μm) by optical lithography and lift-off process. These Ni-Schottky contacts were deliberately not subjected to annealing treatments to avoid interface reactions, which would induce a consumption of the SiC layer and/or a degradation of the barrier properties [28].

The Schottky contacts were characterized by means of current-voltage (I-V) measurements, under both forward and reverse bias, at various temperatures in the range 25-115 °C (step of 15 °C). The measurements were performed in a Karl-Suss MicroTec probe station equipped with a parameter analyzer.

3. Results and Discussion

Firstly, Fig.1 compares the forward room-temperature current density-voltage (J-V_F) characteristics of Ni Schottky contacts formed on an n-type 4H-SiC epilayer, with or without a heavily-doped n-type implanted layer.

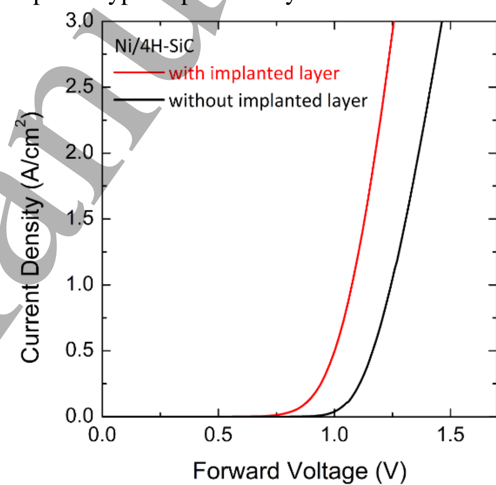

Figure 1. Forward J-V_F characteristics of Ni Schottky contacts on an n-type 4H-SiC epilayer, with or without a heavily-doped n-type implanted layer.

As one can see, the J-V_F curve of the contact on the heavily-doped n-type implanted 4H-SiC exhibts a lower turn-on voltage with respect to the reference contact formed on the 4H-SiC epilayer without implant.

Under forward bias, the electrical behavior of 4H-SiC Schottky diodes is typically described by the thermionic emission (TE) model [29,30,31], with the current density-voltage (J_{TE} -V_F) relationship expressed by:

$$J_{TE} = A^{*}T^{2} \times exp\left(-\frac{q\phi_{B_{TE}}}{k_B T}\right) \times \exp\left(q\,\frac{V_F - J_{TE}R_{on}}{nk_B T}\right) \quad (1)$$

where A^* is the effective Richardson's constant of 4H-SiC (146 A·cm^{-2}·K^{-2}) [32], k_B = 1.38× 10^{-23} J/K is the Boltzmann's constant, q is the elementary charge, V_F is the voltage applied across the metal/semiconductor interface and

Accepted Manuscript

T is the absolute temperature. The relevant diode parameters in Eq. (1), i.e., ideality factor n, Schottky barrier height Φ_{BTE} and specific on-resistance R_{ON}, were derived as best fit parameters. The experimental value of barrier height measured in Ni-Schottky contacts on 4H-SiC epitaxial layer) typically ranges between 1.3 - 1.6 eV [10,33,34,35].

In our case, Ni Schottky contacts fabricated directly on the 4H-SiC epilayer (without implanted layer, black curve in Fig.1) resulted in a barrier height of 1.32 eV,determined by using the TE model.

On the other hand, the TE model applied to the Ni Schottky contacts on the heavily-doped n-type implated layer gave a barrier height Φ_{BTE} = 0.94 eV and an ideality factor n = 1.8. Such a strong discrepancy with respect to the ideal behavior (n=1) suggests that the current transport at the Ni/heavily-doped 4H-SiC interface cannot be described by a pure TE regime. More reasonably, considering the high doping concentration of the implanted region, the presence of a tunneling contribution to the forward current transport must be taken into account. Thus, for analyzing the forward characteristic we considered a thermionic field emission (TFE) model [36,37], that is a thermal-assisted tunneling. Fig. 2 (open symbols) reports the semilog plot of the experimental forward J-V_F characteristic of a representative diode acquired at room temperature with the inset depicted a not to scale schematic energy band diagram of a thermal-assisted tunneling transport. In this scheme, n^+ and n^- represent the implanted and the epitaxial regions, respectively, while E_C and E_F are the bottom of the conduction band and the Fermi level in the semiconductor. The experimental forward characteristics were fitted by the TFE relationship (continuous line in Fig.2), that is expressed by [37]:

$$J_{TFE} = J_{0,TFE}(V_F) \times \exp\left(q\frac{V_F - J_{TFE}R_{on}}{E_0}\right) \quad (2)$$

where the saturation current $J_{0,TFE}$ (V_F) is given by:

$$J_{0,TFE}(V_F) = \frac{A^{**}T}{k_B cosh(qE_{00}/k_BT)} \times \sqrt{\pi E_{00}\left(\phi_{B_{TFE}} - \Delta E_F - (V_F - J_{TFE}R_{ON})\right)} \times \exp\left(-\frac{q\Delta E_F}{k_BT} - \frac{\phi_{B_{TFE}} - \Delta E_F}{E_0}\right) \quad (3)$$

and $E_0 = E_{00} \times coth\left(\frac{qE_{00}}{k_BT}\right)$, with q is the elementary charge, k_B is the Boltzmann's constant and T is the absolute temperature. The parameter E_{00} is dependent on the doping concentration N_D, according to $E_{00} = \frac{h}{4\pi} \times \sqrt{\frac{N_D}{m^*\varepsilon_{SiC}}}$ with m^* =0.38 m_0 the effective mass (m_0 is the electron mass) and ε_{SiC} =9.66 ε_0 the dielectric constant of the semiconductor (ε_0 is the vacuum permittivity) [37,38,39,40], while ΔE_F is the difference between the bottom of the conduction band and the semiconductor Fermi level.

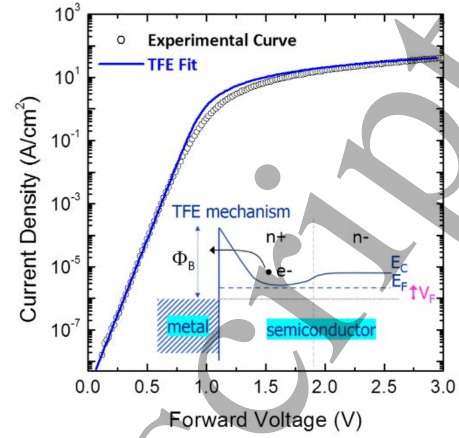

Figure 2. Experimental J-V_F curve (open symbols) for Ni/4H-SiC Schottky diode under forward bias at 25 °C and fitting curve according to the TFE model (continuous line). In the inset, schematic energy band diagram for the metal/4H-SiC contact under forward bias, according to the TFE current transport mechanism.

The barrier Φ_{BTFE} and the doping concentration N_D were determined as parameters of the TFE fit to the experimental J-V_F curve, obtaining Φ_{BTFE} =1.77 eV and N_D=1.97×10^{19} cm^{-3}. The ratio k_BT/qE_{00} gives an indication of the relevance of the thermionic emission process with respect to the tunneling one and allows to evaluate which current transport mechanism is predominant for a given doping concentration [38]. Using N_D=1.97×10^{19} cm^{-3}, the ratio k_BT/qE_{00} is 0.61, which confirms the appropriateness of the TFE model to describe our data.

Furthermore, considering the doping concentration N_D=1.97×10^{19} cm^{-3} derived by the TFE fit, a depletion width W_D =10 nm at the Ni/4H-SiC interface can be estimated at zero bias [41]. Such donor concentration is in agreement with the value measured by scanning capacitance microscopy (SCM) of the active dopant profile on a 4H-SiC sample implanted and annealed under the same conditions [24].

Then, the temperature-dependence of the forward and reverse characteristics of the diode was studied to get additional insights into the dominant current transport mechanisms.

Firstly, the temperature-dependence of the forward J-V_F characteristics was monitored between 25 °C and 115 °C (Fig. 3), showing an increase of the current with the temperature. Specifically, by fitting the experimental curves to TFE model for each temperature, we observed a decrease of the barrier Φ_{BTFE} (from 1.77 to 1.66 eV) with increasing temperature. On the other hand, an almost constant value of doping N_D (1.96±0.02) × 10^{19} cm^{-3} was found as temperature increases, in agreement with our previous Hall measurements carried out on similar samples [24]. The temperature-dependences of the

Accepted Manuscript

barrier height Φ_{BTFE} and the doping concentration N_D are reported as insets in Fig. 3.

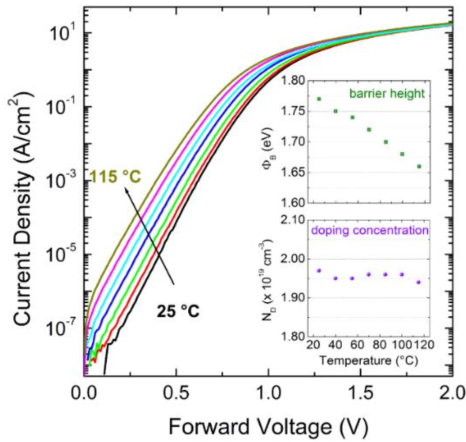

Figure 3. Experimental J-V_F curves for Ni/4H-SiC Schottky diode under forward bias at different measurement temperatures in the range 25-115 °C. The insets show the temperature-dependences of the barrier height and doping concentration values, derived by the TFE fits of the forward J-V_F curves at the different measurement temperatures.

Moreover, as reported in Fig.4, the effective Richardson's constant determined from the plot ln (Is/T^2) vs $1/k_BT$ (where $I_S = AA^*T^2 \times exp\left(-\frac{q\phi_{BTE}}{k_BT}\right)$ is the saturation current of eq. 1), was 4.7×10-4 $A\cdot cm^{-2}\cdot K^{-2}$) . This experimental value is lower than the expected one of 146 $A\cdot cm^{-2}\cdot K^{-2}$ for 4H-SiC [32]. This discrepancy has been often attributed to deviations from the thermionic emission model and/or to lateral inhomogeneity of the barrier [32,42].

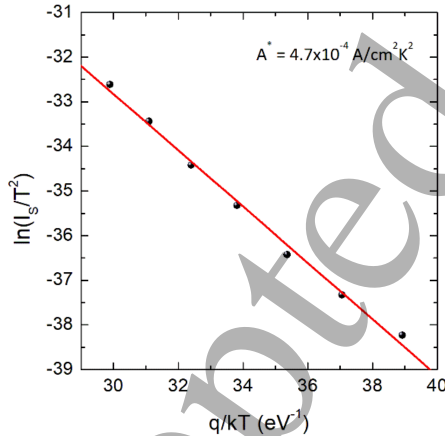

Figure 4: Richardson's plot ln (Is/T2) vs 1/kBT for Ni Schottky diode on n-type implanted 4H-SiC. From the linear fit of the effective barrier height and Richardson's constant could be determined.

The J-V_F measurements, reported in Fig. 3, revealed a temperature dependence of the ideality factor, which in turn confirms a deviation from the ideal TE and suggests the formation of an inhomogeneous Schottky barrier. A way to visualize the deviation from the TE behavior is to report a plot of nkT as a function of kT, as shown in Fig. 5. In particular, besides our experimental data (black open circles), this graph reports also the ideal TE case with n=1 and the case of an inhomogeneous Schottky barrier described by the so-called "T_0 anomaly", with T_0 values typically observed in Schottky contact to 4H-SiC, i.e. varying in a range between 20 and 40 K [43,44,45]. Moreover, in the same graph the nkT *vs* kT curves, calculated with the TFE model for three different doping concentration values, are also reported. As can be seen, an excellent agreement between our experimental data and the calculated TFE curve is obtained for a concentration of $1.96\times10^{19}cm^{-3}$.

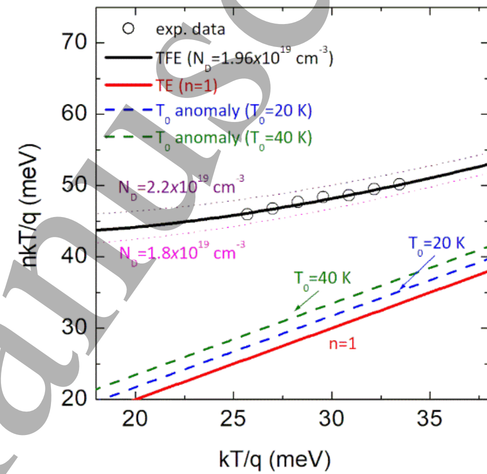

Figure 5: nkT *vs* kT plot for the ideal case n=1 (red solid line), for an inhomogeneous barrier described by the "T_0 anomaly" (dashed lines) and for our experimental data (black open circles). The nkT *vs* kT curves calculated with the TFE for three different doping concentration values are also reported.

Fig. 6a reports the reverse current density-voltage characteristic (J-V_R) of the Ni/4H-SiC Schottky diode acquired at various temperatures. As can be seen, the reverse current density increases from tenths of nA/cm^2 up to some units of A/cm^2 with increasing reverse bias. Noticeably, while the reverse current exhibits a clear dependence on the measurement temperature for lower voltage, it becomes almost independent of the temperature at higher bias values.

The field emission (FE) regime through a metal/semiconductor interface predicts only a weak temperature dependence of the reverse current, with the reverse current density expressed as [37]

$$J_{FE}(V_R) = \frac{qA^{**}T^2\pi E_{00}\times exp\left(-\frac{2\phi_b{}^{3/2}}{3E_{00}(\phi_B-V_R)^{1/2}}\right)}{k_BT[\phi_B/(\phi_B-V_R)]^{1/2}sin\{\pi k_BT[\phi_B/(\phi_B-V_R)]^{1/2}/E_{00}\}} \quad (4)$$

with the meaning of symbols as mentioned above.

Accepted Manuscript

At room temperature (inset of Fig. 6a), the FE model could fit the experimental data with a barrier height Φ_B=1.77e V and a doping concentration N_D=1.0×10^{19}cm^{-3}. In this case, an effect of the series resistance at high current level (high reverse voltage) cannot not be ruled out. Moreover, the FE model could not well describe the experimental curves at all measurement temperatures. Hence, it is possible to argue that an additional mechanism must be taken into account to explain the more pronounced temperature behaviour of the reverse current at low voltage.

Fig. 6b reports an Arrhenius' plot of the current density for three representative reverse biases (at 1V, 3V and 8V). From these plots, it was possible to determine the activation energy E_A that varies from of 0.387eV at 1V down to 0.205eV at 3V. Interestingly, the Arrhenius' plot gives a much lower activation energy of 0.052eV at 8V, where the current is almost independent of temperature. This latter is consistent with the prevalence of a tunnelling mechanism coexisting with the series resistance contribution of the epilayer. In fact, since the FE is almost independent of temperature, the activation energy determined from the Arrhenius' plot of the leakage current significantly decreases with increasing the reverse bias, i.e. where FE becomes dominant.

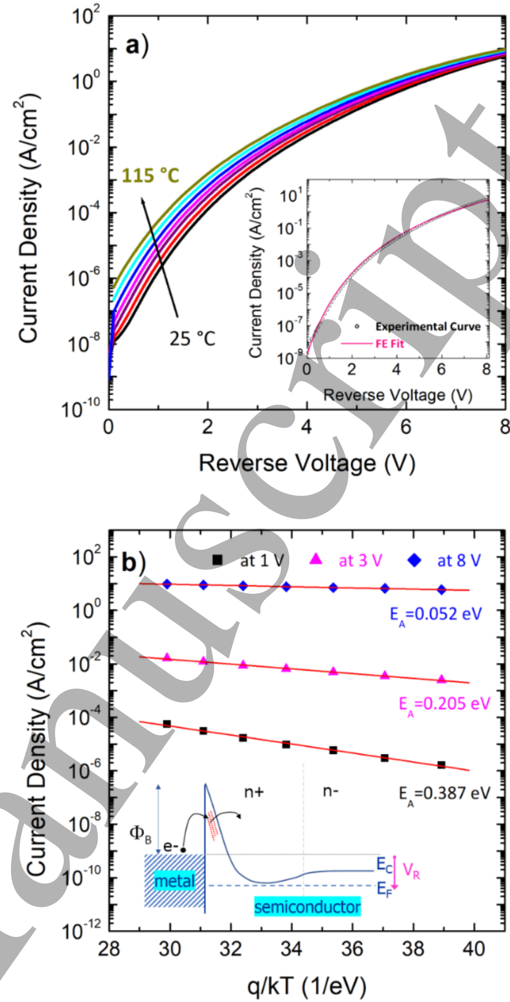

Figure 6. (a) Experimental J-V_R characteristics of the Ni/4H-SC contact under reverse bias in the temperature range 25-115 °C. The inset reports the reverse characteristic acquired at room temperature (open symbols) and the fitting curve according to the FE regime (continuous line). (b) Arrhenius' plot of the current density at three different biases (1V, 3V and 8V), giving activation energy E_A of 0.387eV at 1V and 0.205eV at 3V; the current is almost independent of the temperature at 8V. In the inset, schematic energy band diagram for trap-assisted tunneling contribution to the current transport under moderate reverse bias.

As observed in literature [36,46,47,48,49,50,51], a large variety of defects can be induced in 4H-SiC by ion-implantation and post thermal treatments, introducing energy levels within the band gap of the material, which can have an impact on the leakage current of Schottky diodes. Plausibly, the defects in our high dose P-ion implanted sample induce energy levels that can assist the current transport in the moderate reverse bias range, explaining the temperature-

Accepted Manuscript

dependence of the reverse characteristics (inset Fig.6b). At higher voltages, the direct tunneling FE becomes progressively dominant, due to the barrier thickness reduction.

A possible application of these results in a real device was considered by performing a numerical simulation of the potential distribution in a JBS diode structure. The JBS consists in embedding p^+-type regions (usually achieved by ion implantation) within an n-type Schottky area. In this layout, the leakage current of the Schottky contact on a n^+-doped surface region can be mitigated by the lateral depletion of the p^+-n junctions. The numerical simulation, carried out using a drift diffusion solver implemented in the open source FEniCS platform [52] and employing a heavily doped n^+-type region below the Schottky metal, is shown in Fig. 7 for a reverse bias of -10V. FEniCS allows accurate and robust implementation of user defined coupled partial differential models, as the drift-diffusion one, whilst an efficient computer aided design (CAD) of the structure and the meshing algorithm is obtained coupling the FEniCS python modules with the Gmsh package (again in open source licensing format) [53]. The JBS structure (inset of Fig. 7) assumes ideally 0.6 μm-thick rectangular p^+-regions ($N_A = 2\times 10^{19}$ cm^{-3}) placed around a 1.4 μm wide Schottky contact formed on a thin 50 nm n^+-region ($N_D = 1\times 10^{19}$ cm^{-3}) over a n- drift layer ($N_D = 1\times 10^{16}$ cm^{-3}). The experimental value of the Schottky barrier height is used on the n^+-region, while ohmic contacts are assumed in the p^+- regions.

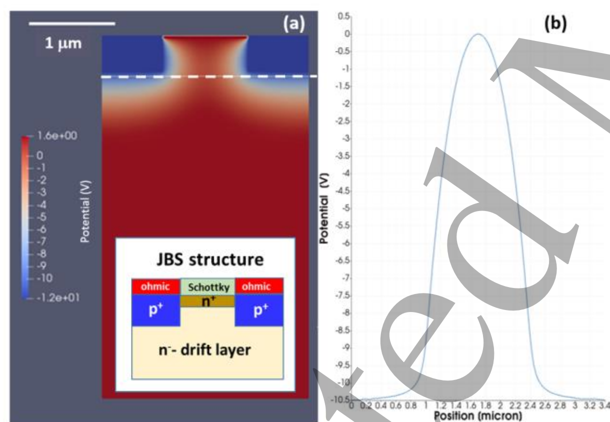

Figure 7. (a) Numerical study of the potential distribution for a JBS structure (schematically depicted in the inset) employing a heavily doped n^+-type region below the Schottky metal, for a reverse bias of -10V. The potential reference in the bulk n- epi region is aligned to its quasi-Fermi energy. (b) Cut line of the potential distribution 50nm above the p^+-regions, showing the pinch-off effect.

Evidently, a full depletion (pinch-off) of the region below the Schottky metal is generated by the p^+/n^- lateral junction under this reverse bias condition, which should suppress the leakage current of the device, by reducing the effective conduction channel width for the carriers emitted from the Schottky contact.

Obviously, this action is gradual with increasing the reverse bias, with an overall benefit on the diode features. On the other hand, the lower turn-on voltage under forward bias guarantees a low power consumption compared to the case of a conventional JBS structure without the n^+-type region below the Schottky contact.

It is worth noting that in such conventional devices, the pinch-off condition can be achieved already at a lower reverse bias (≈ -6V). However, with an appropriate device layout (i.e., width of the Schottky and Ohmic regions), the proposed method can be promising to control the barrier in JBS diodes.

4. Conclusions

In conclusion, the electrical behavior of a Ni Schottky barrier formed onto heavily ($N_D > 10^{19}$ cm^{-3}) doped n-type implanted 4H-SiC was investigated, elucidating the current transport mechanisms in both forward and reverse bias. An accurate analysis of the current transport showed that current injection in forward bias is described by a thermionic-field emission mechanism. Under reverse bias, the temperature behavior of the leakage current is affected by the presence of implantation-induced damage at low bias, while a pure field emission mechanism is approached with increasing the bias. A numerical study of the potential distribution in a JBS diode demonstrated the possibility to apply this process to improve the performance of real 4H-SiC Schottky

Acknowledgements

The authors would like to acknowledge STMicroelectronics for providing 4H-SiC implanted samples and S. Di Franco (CNR-IMM) for technical assistance in the diodes fabrication. Part of this research activity has been carried out in the framework of the European ECSEL JU project REACTION (Grant Agreement No. 783158), using the facilities of the Italian Infrastructure Beyond-Nano.

References

[1] Ren F, Zolper J C, Wide Energy Bandgap Electronic Devices, World Scientific Publishing Co. Pte. Ltd., Singapore (2003).

[2] Kassakian G and Johns T M 2013 *IEEE J. Emerg. Sel. Topics Power Electron.* **1** 47

Accepted Manuscript

1
2
3
4
5
6
7
8
9
10
11
12
13
14
15
16
17
18
19
20
21
22
23
24
25
26
27
28
29
30
31
32
33
34
35
36
37
38
39
40
41
42
43
44
45
46
47
48
49
50
51
52
53
54
55
56
57
58
59
60

[3] Roccaforte F, Giannazzo F, Iucolano F, Eriksson J, Weng MH and Raineri V 2010 *Appl. Surf. Sci.* **256** 5727
[4] Kimoto T 2015 *Jap. J. Appl. Phys.* **54** 040103
[5] Friedrichs P 2008 *Phys. Stat. Sol. B* **245** 1232
[6] She X, A. Q. Huang, O. Lucìa, and B. Ozpineci, IEEE Transactions Ind. Electron. 64, 8193 (2017).
[7] Roccaforte F, Fiorenza P, Greco G, Lo Nigro R, Giannazzo F, Iucolano F and Saggio M 2018 *Microelectronic Engineering* **187–188** 66
[8] Pristavu G, Brezeanu G, Pascu R, Drăghici F and Bădilă M 2019 *Mater. Sci. Semicond. Process* **94** 64
[9] Sciuto A, Roccaforte F and Raineri V 2008 *Appl. Phys. Lett.* **92** 0935050
[10] Roccaforte F, Brezeanu G, Gammon P M, Giannazzo F, Rascunà S and Saggio M 2018 *Schottky Contacts to Silicon Carbide: Physics, Technology and Applications, in Advancing Silicon Carbide Electronics Technology I, Materials Research Foundations* **37** pp. 127-190. (http://dx.doi.org/10.21741/9781945291852-3).
[11] Yakimova R, Hemmingsson C, MacMillan M F, Yakimov T and Janzén E 1998 *J. Electron. Mater.* **27** 871
[12] Weiss R, Frey L and Ryssel H 2001 *Appl. Surf. Sci.* **184** 413
[13] Gora V E, Chawanda C, Nyamhere C, Auret F D, Mazunga F, Jaure T, Chibaya B, Omotoso E, Danga H T and Tunhuma S M 2018 *Physica B* **535** 333
[14] Stöber L, Konrath J P, Patocka F, Schneider M and Schmid U 2016 *IEEE Trans. Electron Dev.* **63** 578
[15] Huang L and Gu X 2019 *J. Appl. Phys.* **125** 025301
[16] Renz A B, Shah V A, Vavasour O J, Bonyadi Y, Li F, Dai T, Baker G W C, Hindmarsh S, Han Y, Walker M, Sharma Y, Liu Y, Raghothamachar B, Dudley M, Mawby P A and Gammon P M 2020 *J. Appl. Phys.* **127** 025704
[17] Roccaforte F, Bongiorno C, La Via F and Raineri V 2004 *Appl. Phys. Lett.* **85** 6152
[18] Tung R T 2014 *Appl. Phys. Rev.* **1** 011304.
[19] Hara M, Kaneko M and Kimoto T 2021 *Jpn. J. Appl. Phys.* **60** SBBD14.
[20] Triendl F, Pfusterschmied G, Schwarz S, Pobegen G, Konrath J P and Schmid U 2021 *Semicond. Sci. Technol.* **36**, 055021.
[21] Berthou M, Godignon P, Montserrat J, Millan J and Planson D 2011 *J. Electron. Mater.* **40** 2355.
[22] Pérez R, Mestres N, Vellvehi M, Godignon P and MillanJ 2006 *Semicond. Sci. Technol.* **21** 670.
[23] Vivona M, Greco G, Giannazzo F, Lo Nigro R, Rascunà S, Saggio M and Roccaforte F 2014 *Semicond. Sci. Technol.* **29** 075018.
[24] Spera M, Greco G, Severino A, Vivona M, Fiorenza P, Giannazzo F and Roccaforte F 2020 *Appl. Phys. Lett.* **117** 013502
[25] Hara M, Asada S, Maeda T and Kimoto 2020 T, *Appl. Phys. Express* **13** 041001
[26] Severino A, Mello D, Boninelli S, Roccaforte F, Giannazzo F, Fiorenza P, Calabretta C, Calcagno L, Piluso N and Arena G 2019 *Mater. Sci. Forum* **963** 407
[27] Frazzetto A, Giannazzo F, Lo Nigro R, Raineri V and Roccaforte F 2011 *J. Phys. D.: Appl. Phys.* **44** 255302
[28] Calcagno L, Ruggiero A, Roccaforte F and La Via F 2005 *J. Appl. Phys.* **98** 023713
[29] Rhoderick E 1982 *IEEE Proc.* **129** 1
[30] Nicholls J, Dimitrijev S, Tanner P and Han H 2019 *Sci. Rep.* **9** 3754
[31] Türüt A. 2020 *Turkish J. Phys.* **44** 302
[32] Roccaforte F, La Via F, Raineri V, Pierobon R and Zanoni E 2003 *J. Appl. Phys.* **93** 9137
[33] Itoh A and Matsunami H 1997 *Phys. Status Solidi* **162** 389
[34] Kestle A, Wilks S P, Dunstan P X, Prilcliard M and Mawby P A 2000 *Electron. Lett.* **36** 267
[35] Aydın M E, Yıldırım N and Türüt A 2020 *J. Appl. Phys.* **102** 043701
[36] Kimoto T and Cooper J A 2014 Fundamentals of Silicon Carbide Technology, Ed. John Wiley & Sons Singapore Pte. Ltd
[37] Padovani F A and Stratton R 1966 *Solid-State Electron.* **9** 695
[38] Pensl G, Ciobanu F, Frank M, Krieger M, Reshanov S, Schmid F, Weidner M 2006 "*SiC-Materials and Devices", Selected Topics in Electronics and Systems* **40** Shur M, Rumyantsev S and Levinshtein M Edt., pp.1-41 - World Scientific Publishing Co. Pte. Ltd., Singapore
[39] Yu A Y C 1970 *Solid-State Electron.* **13** 239
[40] Roccaforte F, La Via F and Raineri V 2005 *Int. J. High Speed Electron. Syst.* **15** 781
[41] Sze S M 2001 *Semiconductor Devices: Physics and Technology, 2nd ed., Wiley, New York*
[42] Brezeanu G, Pristavu G, Draghici F, Badila M and Pascu R 2017 *J. Appl. Phys.* **122** 084501
[43] Sullivan J P, Tung R T, Pimto M R and Graham W R 1998 *J. Appl. Phys.***70** 7403
[44] Ferhat Hamida A, Ouennoughi Z, Sellai A, Weiss R and Ryssel H 2008 *Semicond. Sci. Technol.* **23** 045005
[45] Boussouar L, Ouennoughi Z, Rouag N, Sellai A, Weiss R, Ryssel H 2011 *Microelectr. Eng.* **88** 969
[46] Dalibor T, Pensl G, Matsunami H, Kimoto T, Choyke W J, Schöner A and Nordell N 1997 *Phys. Stat. Sol. A* **162** 199
[47] Hallén A, Henry A, Pellegrino P, Svensson B G and Åberg D 1999 *Mater. Sci. Eng. B* **61 – 62** 378
[48] Roccaforte F, Libertino S, Raineri V, Ruggiero A, Massimino V and Calcagno L 2006 *J. Appl. Phys.* **99** 013515
[49] Kawahara K, Alfieri G, KimotoT 2009 *J. Appl. Phys.* **106** 013719
[50] Zippelius B, Suda J and Kimoto T 2012 *Mater. Sci. Forum* **717-720** 247
[51] Nipoti R, Ayedh H M and Svensson B G 2018 *Mater. Sci. Semicond. Process.* **78** 13
[52] https://fenicsproject.org/
[53] https://gmsh.info/

Accepted Manuscript